RSC Advances

PAPER

View Article Online
View Journal | View Issue

Cite this: *RSC Adv.*, 2017, **7**, 35147

Transparent $Na_5Gd_9F_{32}:Er^{3+}$ glass-ceramics: enhanced up-conversion luminescence and applications in optical temperature sensors

Xiaoman Li,[ab] Jiangkun Cao,[ab] Fangfang Hu,[a] Rongfei Wei[a] and Hai Guo *[a]

Received 11th June 2017
Accepted 28th June 2017

DOI: 10.1039/c7ra06520e

rsc.li/rsc-advances

New rare earth ion-doped nanocomposite materials, $Na_5Gd_9F_{32}:Er^{3+}$ glass-ceramics, were fabricated *via* a traditional melt-quenching technique and subsequent heat treatments. Their microstructural and optical properties were systemically investigated by XRD, TEM, HRTEM techniques, absorption, up-conversion spectra and luminescence lifetime measurements. Excited by 980 nm laser, both glass and glass-ceramic samples presented characteristic red and green up-conversion emissions of Er^{3+} ions. After crystallization, Er^{3+} ions were incorporated into the precipitated $Na_5Gd_9F_{32}$ nanocrystals. Compared with precursor glasses, the red up-conversion intensity of glass-ceramics was enhanced by 1300 times, and the luminescence lifetime was also prolonged. The fluorescence intensity ratio technique was utilized to carry out the optical thermometry based on the green up-conversion luminescence behavior of Er^{3+} ions. Results manifest that $Na_5Gd_9F_{32}:Er^{3+}$ glass-ceramics would have potential applications in optical temperature sensors with high sensitivity.

Introduction

Fluoride nanocrystal-based oxyfluoride glass-ceramics, a new type of nanocomposite material,[1–18] have received much interest in recent years. Generally, glass-ceramics are fabricated by a traditional melt-quenching technique with subsequent crystallization processes. They are isotropic and possess the ability to be shaped into diverse geometrical structures. By proper heat treatment, one or more crystalline phases can be participated through *in situ* growth in a glass matrix.[19–21] Thus, the advantages of fluoride nanocrystals can be achieved with the merit of glass preserved. That is to say that glass-ceramics combine the high chemical, mechanical and thermal stability of glasses with the low phonon energy and strong crystal field environment of fluoride nanocrystals.[3–17]

Inspiringly, doped rare earth (RE) ions will preferentially get incorporated into the as-synthesized fluoride nanocrystals phase[8–17] and exhibit excellent luminescent behavior, which makes RE ion-doped fluoride glass-ceramics potential candidates for optoelectronic devices, such as in lighting,[22] multicolor displays,[11] sensors[15] and scintillators.[23] In this case, numerous RE fluoride glass-ceramics have been fabricated and explored, such as La, Gd, Yb, Lu and Y-based fluoride glass-ceramics.[13–17,22–26]

The luminescent properties of RE ion-doped fluoride glass-ceramics remarkably depend on the crystalline phase precipitated in glass matrix. The sodium–gadolinium–fluoride compounds ($Na_xGd_yF_{x+3y}$), particularly $NaGdF_4$ and $Na_5Gd_9F_{32}$, are identified as efficient up-conversion hosts for RE ions doping. The fabrication and luminescent properties of RE ion-doped $NaGdF_4$ and $Na_5Gd_9F_{32}$ nanoparticles have frequently attracted attention.[27–30] However, the application of such fluoride nanocrystals is hampered by their insufficient thermal stability leading to phase transition or decomposition during the reheating process.[28–30] Fortunately, this disadvantage may be compensated by integrating $Na_xGd_yF_{x+3y}$ nanocrystals in a glassy matrix considering the good properties of glass-ceramics mentioned above. Numerous investigations on $NaGdF_4$ glass-ceramics have been reported,[3,31] particularly on the up-conversion luminescence behavior of Er^{3+}-doped ones.[3] However, only one report on $Na_5Gd_9F_{32}$ glass-ceramics was published.[32] Therefore, it is promising to investigate whether $Na_5Gd_9F_{32}$ glass-ceramics are thermal stable $Na_xGd_yF_{x+3y}$ compound for RE up-conversion luminescence.

Er^{3+} ions are the most excellent up-conversion luminescent centers[33] exhibiting visible up-conversion luminescence pumped by near-infrared (NIR) laser. They can be used as probes for optical detection of magnetic field.[34] In addition, Er^{3+} ions have a couple of thermally coupled energy levels (TCEL), $^2H_{11/2}$ and $^4S_{3/2}$ levels. As a result, there has been growing interest in the optical thermometry of glass-ceramics doped with Er^{3+} ions,[15,16] since these Er^{3+}-doped glass-ceramics can be used as optical temperature sensors. Moreover, no reports on optical thermometry of Er^{3+}-doped $Na_5Gd_9F_{32}$ glass-ceramics have been

[a]*Department of Physics, Zhejiang Normal University, Jinhua, Zhejiang, 321004, China. E-mail: ghh@zjnu.cn*

[b]*State Key Laboratory of Luminescent Materials and Devices, South China University of Technology, Guangzhou, Guangdong, 510640, China*

published. Therefore, it is incumbent upon us to research the structural, up-conversion luminescent properties and temperature sensing properties of Er^{3+}-doped $Na_5Gd_9F_{32}$ glass-ceramics.

In this study, Er^{3+}-doped novel transparent oxyfluoride glass-ceramics containing $Na_5Gd_9F_{32}$ nanocrystals were fabricated and the unique up-conversion properties of Er^{3+} ions were investigated in detail. No phase transition occurs during different heat treatment processes, which suggests that $Na_5Gd_9F_{32}$ glass-ceramics have better thermal stability than the reported $Na_5Gd_9F_{32}$ nanocrystals.[29] Enhanced up-conversion emissions and prolonged luminescence lifetimes of Er^{3+} ions indicate that Er^{3+} ions have been preferentially incorporated into $Na_5Gd_9F_{32}$ nanocrystals. The optical thermometry results of temperature-dependent green up-conversion spectra suggest that the $Na_5Gd_9F_{32}$ glass-ceramics with high sensitivity can be good candidates for optical temperature sensors.

Experimental

Glass samples with nominal composition $45SiO_2$–$10Na_2CO_3$–$15Al_2O_3$–$4CaCO_3$–$18NaF$–$8GdF_3$–$0.2ErF_3$ (in mol%) were prepared by the melt-quenching method. SiO_2, Al_2O_3, Na_2CO_3, NaF (A.R., all from Sinopharm Chemical Reagent Co., Ltd.), and high-purity GdF_3 and ErF_3 (99.99%, from AnSheng Inorganic Materials Co., Ltd.) were used as starting materials. The well ground stoichiometric chemicals were put into a covered alumina crucible and melted at 1500 °C for 1 h in air atmosphere. The melt was poured onto a 300 °C preheated stainless-steel plate and then pressed by another plate to get solid samples. After annealing at 450 °C for 5 h to release internal stresses, precursor glasses (labelled as PG) were formed. Subsequently, PG were subjected to heat treatment for 2 h at 590 °C, 610 °C and 630 °C to fabricate transparent glass-ceramics, which were labelled as GC590, GC610 and GC630, respectively. All samples were polished optically with a thickness of 2 mm for further characterization.

X-ray diffraction (XRD) patterns were obtained on the Philips X' Pert PRO SUPER X-ray diffraction apparatus (40 kV, 40 mA) with Cu Kα radiation ($\lambda = 0.154056$ nm) over the angular range of $10^\circ \leq 2\theta \leq 80^\circ$ in a step size of 0.0167°. For XRD measurement, the lump glasses were ground to a fine powder in an agate mortar. Transmittance spectra were measured on the U-3900 Ultraviolet-Visible (UV-VIS) spectrophotometer. The microstructure of glass-ceramics was analyzed using the JEM-2100F transmission electron microscope (TEM) operated at an accelerating voltage of 200 kV (JEOL Ltd.). Up-conversion spectra were measured on the FS920 spectrofluorometer (Edinburgh Instruments) with a 980 nm laser (300 mW mm^{-2}) as the excitation source. The spot size of the 980 nm laser was about 1×6 mm^2. In addition, the pump power was adjusted through neutral density filters. The temperature of the sample fixed on a copper post was controlled over the range of 300–510 K by a temperature controller (FOTEK MT48-V-E, Taiwan) with a type-K thermocouple and a heating tube. Decay curve measurements were performed on the SBP500 monochromator (Zolix Instruments) coupled to the Hamamatsu R928 photomultiplier with the Tektronix TDS5052 oscilloscope.

Results and discussion

Fig. 1(a) shows the XRD patterns of PG, GC590, GC610 and GC630 samples. PG does not exhibit any discrete diffraction peaks, confirming its amorphous nature. For GC590, GC610 and GC630 samples, their diffraction peaks match well with those of the cubic $Na_5Gd_9F_{32}$ (JCPDS card no. 27-0698), indicating that cubic $Na_5Gd_9F_{32}$-based glass-ceramics were successfully fabricated. The GC630 sample crystallized at 630 °C still maintains cubic $Na_5Gd_9F_{32}$ phase, indicating that $Na_5Gd_9F_{32}$ glass-ceramics have better thermal stability than nano-sized cubic $Na_5Gd_9F_{32}$ spheres.[29] The size of $Na_5Gd_9F_{32}$ nanocrystals in glass-ceramics can be calculated by the following Scherrer equation:[35]

$$D = k\lambda/\beta \cos\theta \quad (1)$$

where $k = 0.89$, $\lambda = 0.154056$ nm, which represents the wavelength of Cu Kα radiation, θ is the Bragg angle and β represents the corrected half width of diffraction peak. The mean crystalline sizes estimated are about 14, 17 and 24 nm for $Na_5Gd_9F_{32}$ nanocrystals in GC590, GC610 and GC630 (listed in Table 1), respectively.

The transmission spectra of PG, GC590, GC610 and GC630 samples are shown in Fig. 1(b) and the transparence of GC610 sample is up to 74% at 600 nm. The absorption peaks located at 379, 488, 525 and 652 nm are ascribed to the transitions from ground $^4I_{15/2}$ state to $^4G_{11/2}$, $^4F_{7/2}$, $^2H_{11/2}$ and $^4F_{9/2}$ excited states of Er^{3+}, respectively.[14] Photographs and transmittances of PG and all GC samples are given in Fig. 1(e)–(h) and Table 1, respectively. It can be seen that $Na_5Gd_9F_{32}$ glass-ceramics are transparent with excellent uniformity, indicative of homogeneous crystallization of these samples. According to Rayleigh–Gans theory,[5] except for the size of nanocrystals, the difference in refractive index between the crystal phase and the glass phase is also an important parameter for the transmittance of samples. For GC590 and GC610 samples, as the size of the precipitated crystals is much smaller than the wavelength of visible and near-infrared light, glass-ceramics still maintain a good transparency in visible to near-infrared region (Fig. 1(b), (f) and (g)). However, with the increase in heat-treatment temperature, the size of nanocrystals increases to some extent, and the influence of refractive index between the crystal phase and the glass phase plays a more significant role in transmittance from glass-ceramics. Therefore, the transparence of GC630 sample decreased (Fig. 1(b) and (h)) due to the strong light scattering of $Na_5Gd_9F_{32}$ nanocrystals and the large difference in the refractive index between $Na_5Gd_9F_{32}$ crystal phase and glass phase.

TEM and high-resolution TEM (HRTEM) images of GC610 sample are shown in Fig. 1(c) and (d), respectively. TEM bright-field micrograph reveals that $Na_5Gd_9F_{32}$ nanocrystals are homogeneously dispersed in amorphous glassy phase. The corresponding selected area electron diffraction (SAED) patterns

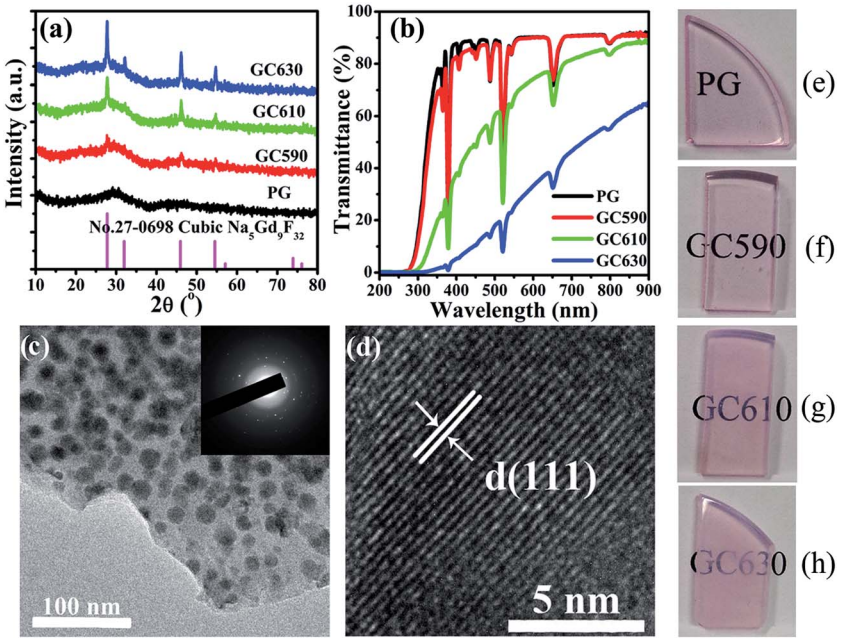

Fig. 1 (a) XRD patterns of PG, GC590, GC610 and GC630 samples, and the reference data of JCPDS card no. 27-0698 for cubic $Na_5Gd_9F_{32}$. (b) Transmission spectra of PG, GC590, GC610 and GC630 samples. (c) TEM and (d) HRTEM images of GC610; the inset is the SAED pattern. Photographs of (e) PG, (f) GC590, (g) GC610 and (h) GC630 samples.

of GC610 sample indicate that glass-ceramics are composite materials that contain amorphous glasses and poly-nanocrystals. The crystal size of $Na_5Gd_9F_{32}$ nanocrystals in GC610 sample is about 17 nm, in accordance with that estimated by the Scherrer equation. The HRTEM image clearly displays the resolved lattice fringes and the value of the associated interplanar spacing d is about 0.333 nm, which corresponds to (111) crystal plane of cubic $Na_5Gd_9F_{32}$ ($d_{(111)} = 0.321$ nm).

The up-conversion spectra ($\lambda_{ex} = 980$ nm, 300 mW mm^{-2}) of PG, GC590, GC610 and GC630 samples are given in Fig. 2(a). Green emission bands (located at 525 and 540 nm) and red emission bands (located at 660 nm) are assigned to $^2H_{11/2}/^4S_{3/2} \rightarrow {}^4I_{15/2}$ and $^4F_{9/2} \rightarrow {}^4I_{15/2}$ transitions of Er^{3+}, respectively.[35] Distinct Stark splitting at 540 and 660 nm in GC samples are observed after crystallization. Moreover, the up-conversion emissions in GC samples are enhanced prominently. Compared with PG, green emissions in GC590, GC610 and GC630 samples enhance by 110, 470 and 1000 times, respectively, whereas red emissions in GC590, GC610 and GC630 samples enhance by 130, 570 and 1300 times (listed in Table 1), respectively. The evident Stark splitting and enhanced up-conversion luminescence may originate due to the incorporation of Er^{3+} ions into cubic $Na_5Gd_9F_{32}$ nanocrystals with variant surroundings of Er^{3+} ions after crystallization, such as changes in symmetry and phonon energy.[5,14]

For the up-conversion process, intensity of up-conversion emission I is proportional to the nth power of pump power density P:[35]

$$I \propto P^n \quad (2)$$

where n is the number of pump photons absorbed per up-converted photon emitted. A plot of log I *versus* log P yields a straight line with slope n. The power dependences of up-conversion of PG and GC610 samples are shown in Fig. 2(b) and (c), respectively. The obtained n values indicate that both red and green up-conversion emissions are caused by two-photon processes.

The excited states for up-conversion can be populated by two famous mechanisms: (1) excited state absorption (ESA) and (2) energy transfer (ET).[35] The ESA process is a single-ion process. Therefore, the rise time of the decay curve of luminescence pumped by the ESA process will be equal to zero. In contrast, the ET process involves two ions, and the ET rate will increase with

Table 1 Synthesized and heat treatment temperature, mean crystalline sizes, up-conversion luminescence and lifetimes of all samples

	Synthesized temperature	Heat treatment temperature	Mean crystalline sizes (nm)	Transmittance at 600 nm	Enhanced factor of red emission (*vs.* PG)	Lifetime of $^4F_{9/2} \rightarrow {}^4I_{15/2}$ transition (ms)
PG	1500 °C, 1 h	—	—	90%	—	0.51
GC590	1500 °C, 1 h	590 °C, 2 h	14	90%	130 times	2.81
GC610	1500 °C, 1 h	610 °C, 2 h	17	74%	570 times	3.58
GC630	1500 °C, 1 h	630 °C, 2 h	24	34%	1300 times	3.80

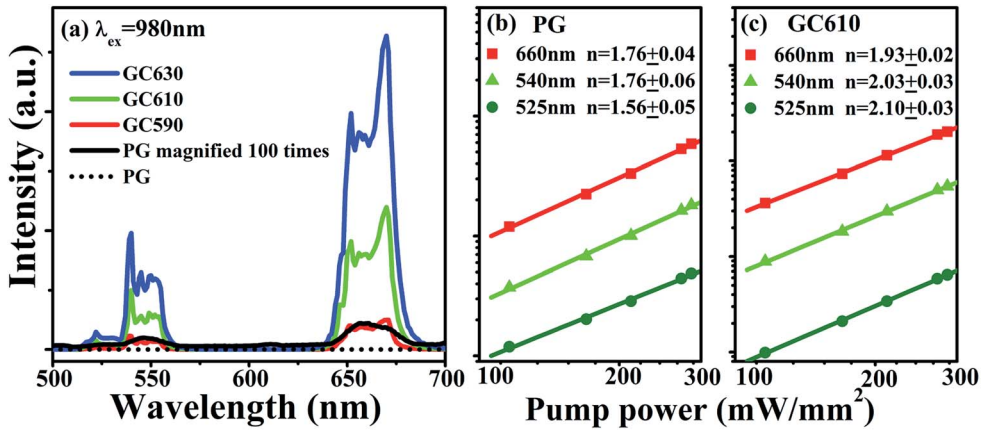

Fig. 2 (a) Up-conversion spectra of PG, GC590, GC610 and GC630 samples; dependence of up-conversion on pump intensity for (b) PG and (c) GC610 samples.

short Er^{3+}–Er^{3+} distances. Hence, the rise time of the decay curve of luminescence pumped by the ET process will be at the same level of lifetime of related metastable levels.

It is well known that glass-ceramics with preferential enrichment of RE ions in the precipitated fluoride nanocrystals can exhibit excellent luminescent behavior and possess a longer lifetime.[14] To further prove the preferential incorporation of Er^{3+} ions into cubic $Na_5Gd_9F_{32}$ nanocrystals and to understand the up-conversion mechanisms more clearly, the decay curves of up-conversion emissions of PG and GC samples were investigated.

Fig. 3(a) shows the decay curves of luminescence at 660 nm ($^4F_{9/2} \rightarrow {}^4I_{15/2}$) emissions of Er^{3+} in PG and GC samples. The lifetimes are characterized by average lifetime ($\bar{\tau}$) derived by[16]

$$\bar{\tau} = \int_0^\infty tI(t)\mathrm{d}t \Big/ \int_0^\infty I(t)\mathrm{d}t \qquad (3)$$

where $I(t)$ is the emission intensity at time t. The average lifetimes of $^4F_{9/2}$ level are about 0.51, 2.81, 3.58 and 3.80 ms for PG, GC590, GC610 and GC630 samples (listed in Table 1), respectively.

Prolonged lifetimes for up-conversion emissions in GC samples indicate the reduced non-radiative relaxation rate of Er^{3+} in GC samples and prove the preferential enrichment of Er^{3+} ions into $Na_5Gd_9F_{32}$ nanocrystals with lower phonon energy. In addition, the rise times at the beginning of decay curves of GC samples are different from that of PG. As shown in Fig. 3(b), the partial magnification of Fig. 3(a), the rise time of PG is almost zero. For all GC samples, the rise times are approximately 0.3 ms for 660 nm emission. Such phenomenon proves that ESA processes are responsible for up-conversion in PG, whereas ET processes are responsible for up-conversion in GC.

In summary, the evident Stark splitting, enhanced characteristic up-conversion emissions and prolonged lifetimes in GC

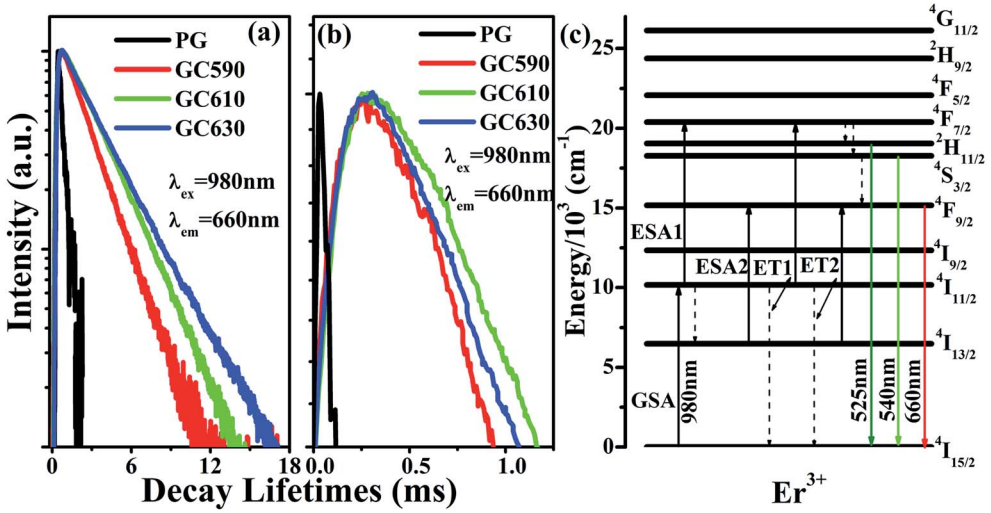

Fig. 3 Decay curves for (a) $^4F_{9/2} \rightarrow {}^4I_{15/2}$ (660 nm) emission of Er^{3+} in PG, GC590, GC610 and GC630 samples (λ_{ex} = 980 nm). (b) The partial enlarged image of (a). (c) Energy level diagram of Er^{3+} and possible up-conversion mechanisms.

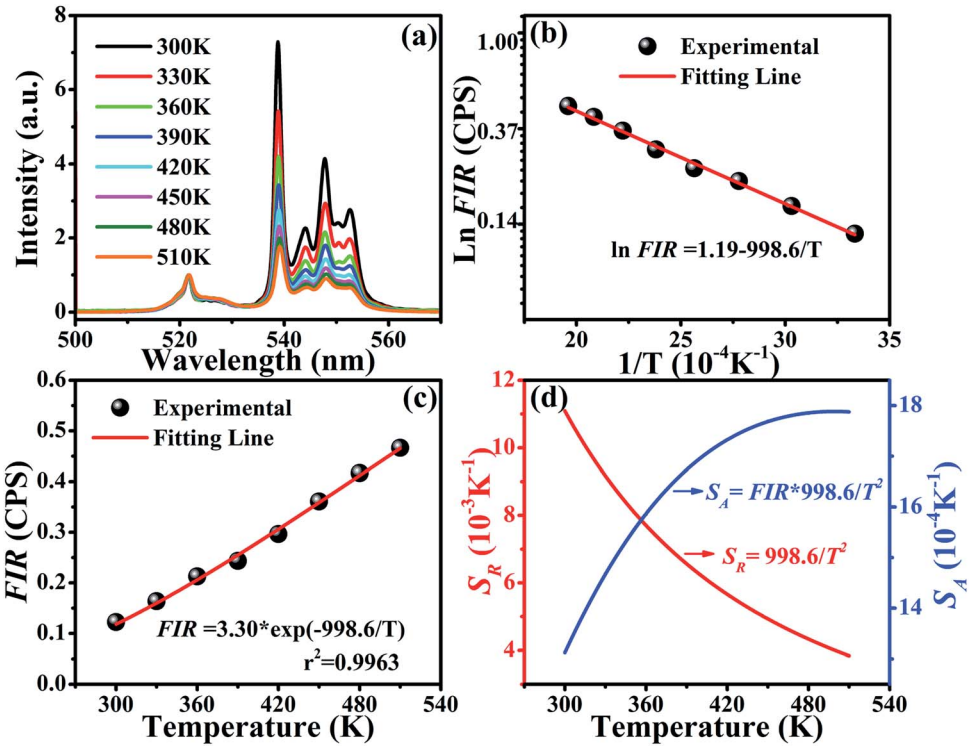

Fig. 4 (a) Green up-conversion spectra of GC630 normalized at 522 nm under the excitation of a 980 nm diode laser at different temperatures from 300 to 510 K. (b) Monolog plot of the FIR as a function of inverse absolute temperature. (c) Temperature dependence of FIR between $^2H_{11/2} \rightarrow {}^4I_{15/2}$ and $^4S_{3/2} \rightarrow {}^4I_{15/2}$ transitions of Er^{3+}. (d) The relative sensitivity S_R and the absolute sensitivity S_A of GC630 under the excitation of a 980 nm diode laser at various temperatures from 300 to 510 K.

samples demonstrate the preferential incorporation of Er^{3+} into $Na_5Gd_9F_{32}$ nanocrystals. In other words, for PG sample, Er^{3+} ions are homogeneously dispersed in glassy phase with long Er^{3+}–Er^{3+} distances. For GC samples, most Er^{3+} ions are incorporated into $Na_5Gd_9F_{32}$ nanocrystals with short Er^{3+}–Er^{3+} distances. The changes in up-conversion spectra are caused by the different surroundings of Er^{3+} ions and the different up-conversion approaches in PG and GC.

On the basis of energy level diagram of Er^{3+} and above discussions, the up-conversion mechanisms accounting for green and red emissions are analyzed and illustrated in Fig. 3(c). Er^{3+} ion is first excited through ground state absorption (Fig. 3(c): GSA) process from $^4I_{15/2}$ level to $^4I_{11/2}$ level by absorbing one 980 nm photon. Subsequently, the ion at $^4I_{11/2}$ level is populated to luminescent levels by different approaches in PG and GC.

For PG sample, ESA processes are dominant because of the longer Er^{3+}–Er^{3+} distances of the homogeneous dispersed Er^{3+} ions in glassy phase. Er^{3+} ion at $^4I_{11/2}$ level absorbs another excitation 980 nm photon and is pumped to $^4F_{7/2}$ level (Fig. 3(c): ESA1).[35] Due to the small energy gap between $^4F_{7/2}$ level and $^2H_{11/2}$, $^4S_{3/2}$ levels, Er^{3+} ion at $^4F_{7/2}$ level can easily and non-radiatively relax to the relatively stable $^2H_{11/2}$ and $^4S_{3/2}$ levels and then produce green up-conversion emissions. The red up-conversion emitting $^4F_{9/2}$ level can be pumped by the following two processes: one is the non-radiative relaxation from the excited $^4S_{3/2}$ state[11,35] and the other is that Er^{3+} absorbs a second 980 nm photon from $^4I_{13/2}$ level (Fig. 3(c): ESA2).[11]

However, for GC samples, ET processes are primarily responsible for up-conversion emission attributing to the fact that Er^{3+} ions incorporate into $Na_5Gd_9F_{32}$ nanocrystals preferentially with shorter Er^{3+}–Er^{3+} distances, lower phonon energy environment and higher crystallization degree. These advantages will reduce the multi-phonon non-radiative relaxation rate and result in enhanced up-conversion luminescence (1300 times).[6] Green luminescent levels can be pumped as follows: an excited Er^{3+} ion at $^4I_{11/2}$ level relaxes to $^4I_{15/2}$ level non-radiatively and transfers its excitation energy to a neighboring Er^{3+} ion at the same level, promoting the latter to $^4F_{7/2}$ level: $^4I_{11/2} + {}^4I_{11/2} \rightarrow {}^4I_{15/2} + {}^4F_{7/2}$ (Fig. 3(c): ET1).[35] Red luminescent $^4F_{9/2}$ level can be populated by the well-known ET2 process: $^4I_{11/2} + {}^4I_{13/2} \rightarrow {}^4I_{15/2} + {}^4F_{9/2}$.[35]

The enhanced up-conversion luminescence and good thermal stability (mentioned in XRD analyses) make $Na_5Gd_9F_{32}$ glass-ceramics promising for highly sensitive optical thermometry. As for optical thermometry, there are three main optical techniques: fluorescence lifetime, amplified spontaneous emissions and fluorescence intensity ratio (FIR) techniques.[15,36–38] Compared with the former two, FIR technique has improved measurement accuracy and widened operating temperature range. It is built on the temperature dependence of the FIR value of transitions from TCEL. Detailed FIR technique can be found in our previous study.[16] FIR technique can reduce the dependence on measurement conditions and has been considered as a promising approach for temperature sensing.

In this case, the temperature-dependent green up-conversion spectra of Er^{3+}-doped $Na_5Gd_9F_{32}$ glass-ceramics were measured by the FIR value of the TCEL ($^2H_{11/2}$ and $^4S_{3/2}$).[39] Fig. 4(a) depicts the normalized green up-conversion spectra (normalized at 522 nm) of GC630 sample measured at different temperatures from 300 to 510 K excited by 980 nm laser with a pump power density of 20.6 mW mm^{-2}. It is clear that the relative intensity ratio of $^2H_{11/2} \rightarrow {}^4I_{15/2}$ transition *versus* $^4S_{3/2} \rightarrow {}^4I_{15/2}$ transition increases monotonously with the elevation in temperature. This is because the population of the $^2H_{11/2}$ and $^4S_{3/2}$ levels of Er^{3+} ion are thermally coupled, and their populations are in accordance with the Boltzmann distribution law. Moreover, the overlap between these two emission bands is small and can be ignored, which favors the measurement accuracy of emission intensities. Both of these characteristics make $Na_5Gd_9F_{32}$:Er^{3+} glass-ceramics potential probes for temperature sensing.

Fig. 4(b) presents the monolog plot of the FIR value of emissions from $^2H_{11/2}$ and $^4S_{3/2}$ as a function of inverse absolute temperature in the range of 300–510 K. The experimental data are fitted to a straight line with the slope of about −998.6. Fig. 4(c) illustrates the temperature dependence of the FIR value in the range of 300–510 K for GC630 sample, and the curve can be well fitted with the following equation:[16,25]

$$\mathrm{FIR} = B\exp(-\Delta E/K_B T) = 3.30\exp(-998.6/T) \quad (4)$$

where B is the pre-exponential parameter; ΔE is the effective energy gap between $^2H_{11/2}$ and $^4S_{3/2}$; K_B is the Boltzmann constant and T is the absolute temperature. According to the fitting results, the effective energy gap ΔE between $^2H_{11/2}$ and $^4S_{3/2}$ levels of Er^{3+} ion can be obtained with a value of 695 cm^{-1}. It is known that the relative sensitivity S_R and the absolute sensitivity S_A are two important parameters to evaluate the property of the sensors for temperature sensing.[16] Thus, the S_R and S_A of GC630 sample are investigated and their fitting results as a function of temperature from 300 to 510 K are described in Fig. 4(d). The calculated S_R value is $998.6/T^2$% K^{-1}. In addition, the S_A value increases with the temperature and is up to the maximum of 17.9×10^{-4} K^{-1} at 499.3 K. Such high sensitivity indicates that $Na_5Gd_9F_{32}$:Er^{3+} glass-ceramics may be used as optical temperature sensors.

Conclusions

Er^{3+}-doped transparent $Na_5Gd_9F_{32}$-based glass-ceramics were successfully fabricated by the melt-quenching method with subsequent crystallization processes. Phase transition did not occur with the increasing heat treatment temperature, which certified the good thermal stability of $Na_5Gd_9F_{32}$ glass-ceramics. The evident Stark splitting, enhanced characteristic up-conversion emissions (1300 times for red emission, 1000 times for green emission), slower rise time and prolonged luminescence lifetime in glass-ceramics reveal the preferential incorporation of Er^{3+} into $Na_5Gd_9F_{32}$ nanocrystals with low phonon energy and shorter Er^{3+}–Er^{3+} distances after crystallization. ESA and ET processes are dominant up-conversion mechanisms in PG sample and GC samples, respectively. The analyses of temperature-dependent green up-conversion manifest the thermal-stable $Na_5Gd_9F_{32}$ glass-ceramics, as novel up-conversion functional materials, may have prospects for optical temperature sensors in the future.

Acknowledgements

This study was supported by the National Natural Science Foundation of China (Grant No. 11374269).

Notes and references

1 C. G. Lin, C. Bocker and C. Rüssel, *Nano Lett.*, 2015, **15**, 6764–6769.
2 S. Liu, D. Q. Chen, Z. Y. Wan, Y. Zhou, P. Huang and Z. G. Ji, *RSC Adv.*, 2016, **6**, 71176–71187.
3 F. X. Xin, S. L. Zhao, L. H. Huang, D. G. Deng, G. H. Jia, H. P. Wang and S. Q. Xu, *Mater. Lett.*, 2012, **78**, 75–77.
4 Z. Y. Zhao, C. Liu, M. L. Xia, Q. Y. Yin, X. J. Zhao and J. J. Han, *J. Alloys Compd.*, 2017, **701**, 392–398.
5 X. S. Qiao, X. P. Fan, J. Wang and M. Q. Wang, *J. Non-Cryst. Solids*, 2005, **351**, 357–363.
6 W. Xu, X. Y. Gao, L. J. Zheng, Z. G. Zhang and W. W. Cao, *Opt. Express*, 2012, **20**, 18127–18137.
7 Y. P. Tai, H. Y. Wang, H. Wang and J. T. Bai, *RSC Adv.*, 2016, **6**, 4085–4089.
8 D. Q. Chen, Y. S. Wang, Y. Yu and P. Huang, *Appl. Phys. Lett.*, 2007, **91**, 051920.
9 D. Q. Chen, Y. Yu, Y. S. Wang, P. Huang and F. Weng, *J. Phys. Chem. C*, 2009, **113**, 6406–6410.
10 F. Lahoz, *Opt. Lett.*, 2008, **33**, 2982–2984.
11 F. Liu, E. Ma, D. Q. Chen, Y. Yu and Y. S. Wang, *J. Phys. Chem. B*, 2006, **110**, 20843–20846.
12 Y. Kawamoto, R. Kanno and J. Qiu, *J. Mater. Sci.*, 1998, **33**, 63–67.
13 A. De Pablos Martín, M. O. Ramírez, A. Durán, L. E. Bausá and M. J. Pascual, *Opt. Mater.*, 2010, **33**, 180–185.
14 X. M. Li, H. Guo, Y. Wei, Y. Guo, H. Lu, H. M. Noh and J. H. Jeong, *J. Lumin.*, 2014, **152**, 168–171.
15 S. Jiang, P. Zeng, L. Q. Liao, S. F. Tian, H. Guo, Y. H. Chen, C. K. Duan and M. Yin, *J. Alloys Compd.*, 2014, **617**, 538–541.
16 X. M. Li, J. K. Cao, Y. L. Wei, Z. R. Yang and H. Guo, *J. Am. Ceram. Soc.*, 2015, **98**, 3824–3830.
17 Y. L. Wei, X. Y. Liu, X. N. Chi, R. F. Wei and H. Guo, *J. Alloys Compd.*, 2013, **578**, 385–388.
18 S. Jiang, H. Guo, X. T. Wei, C. K. Duan and M. Yin, *J. Lumin.*, 2014, **152**, 195–198.
19 C. X. Li, S. Q. Xu, R. G. Ye, S. L. Zhao, D. G. Deng and S. L. Zhuang, *Chin. Opt. Lett.*, 2010, **8**, 66–69.
20 P. F. Li, M. Y. Peng, L. Wondraczek, Y. Q. Zhao and B. Viana, *J. Mater. Chem. C*, 2015, **3**, 3406–3415.
21 M. Y. Peng, D. P. Chen, J. R. Qiu, X. W. Jiang and C. S. Zhu, *Opt. Mater.*, 2007, **29**, 556–561.
22 R. L. Leonard, A. R. Lubinsky and J. A. Johnson, *J. Am. Ceram. Soc.*, 2017, **100**, 1551–1560.

23 J. K. Cao, W. P. Chen, L. P. Chen, X. Y. Sun and H. Guo, *Ceram. Int.*, 2016, **42**, 17834–17838.
24 J. P. Zhang, D. C. Yu, F. F. Zhang, M. Y. Peng and Q. Y. Zhang, *Opt. Mater. Express*, 2014, **4**, 111–120.
25 J. K. Cao, X. M. Li, Z. X. Wang, Y. L. Wei, L. P. Chen and H. Guo, *Sens. Actuators, B*, 2016, **224**, 507–513.
26 G. Krieke, A. Sarakovskis and M. Springis, *J. Alloys Compd.*, 2017, **694**, 952–958.
27 Y. Liu, D. Tu, H. Zhu, R. Li, W. Luo and X. Chen, *Adv. Mater.*, 2010, **22**, 3266–3271.
28 C. Liu, H. Wang, X. Zhang and D. Q. Chen, *J. Mater. Chem.*, 2009, **19**, 489–496.
29 J. Xu, S. Gai, P. a. Ma, Y. Dai, G. Yang, F. He and P. Yang, *J. Mater. Chem. B*, 2014, **2**, 1791–1801.
30 J. Yang, W. Huang, Y. Cheng, C. Wang, Y. Zhao, L. Zhu and X. Cao, *CrystEngComm*, 2012, **14**, 899–907.
31 A. Herrmann, M. Tylkowski, C. Bocker and C. Rüssel, *Chem. Mater.*, 2013, **25**, 2878–2884.
32 D. Q. Chen, Z. Y. Wan, Y. Zhou, Y. Chen, H. Yu, H. W. Lu, Z. G. Ji and P. Huang, *J. Alloys Compd.*, 2015, **625**, 149–157.
33 J. B. Zhao, X. L. Zheng, E. P. Schartner, P. Ionescu, R. Zhang, T. L. Nguyen, D. Y. Jin and H. Ebendorff-Heidepriem, *Adv. Opt. Mater.*, 2016, **4**, 1507–1517.
34 V. K. Tikhomirov, L. F. Chibotaru, D. Saurel, P. Gredin, M. Mortier and V. V. Moshchalkov, *Nano Lett.*, 2009, **9**, 721–724.
35 H. Guo, N. Dong, M. Yin, W. Zhang, L. Lou and S. Xia, *J. Phys. Chem. B*, 2004, **108**, 19205–19209.
36 B. R. Reddy, I. Kamma and P. Kommidi, *Appl. Opt.*, 2013, **52**, B33–B39.
37 K. Z. Zheng, Z. Y. Liu, C. J. Lv and W. P. Qin, *J. Mater. Chem. C*, 2013, **1**, 5502–5507.
38 P. Du, L. H. Luo, W. P. Li, Q. Y. Yue and H. B. Chen, *Appl. Phys. Lett.*, 2014, **104**, 152902.
39 P. Du, L. H. Luo and J. S. Yu, *RSC Adv.*, 2016, **6**, 94539–94546.